Design Study of a High-power Ka-band High-Order-Mode Multi-Beam Klystron

J.C. Cai, I. Syratchev, G. Burt.

Abstract—**Compactness and cost-effectiveness are two major concerns in the development of a Ka-band linearizer, which is a crucial accelerator component of the European CompactLight project. A higher order mode (HOM) Multi-beam Klystron (MBK) could accommodate a higher distributed electron current with a low operating voltage of 60 kV, thus making it competitive to deliver high RF power at high frequency compared with a single beam Klystron or a fundamental mode MBK. In this paper, the modelling and design study of the 36GHz HOM MBK is presented. The development of a double compression multi beam optics system is also elaborated in this paper. The performance validation of such a device was done using sophisticated 3D Particle-In-Cell computer simulations of the entire device. PIC simulations confirmed that a power level of 2.5 MW is attainable with an efficiency of 35 %.**

Index Terms—**Modelling, Optimization, HOM, MBK.**

I. INTRODUCTION

The European CompactLight Project relies on high gradient X-band acceleration technology to drive the X-ray FEL, aiming to make such facilities more affordable to build and operate [1]. In order to minimize the bunch length in the FEL, a magnetic chicane is used as a bunch compressor. In this chicane, the linear chirp of the bunch longitudinal energy profile is designed in a way, that the electrons at the front should take a longer path than the electrons at the back of the bunch. The RF frequency of the injector is chosen to be 6 GHz (a sub-harmonic of the main linac frequency). To provide the necessary linearization in the bunch phase space, a special accelerating cavity, called a linearizer, is used. For a fixed beam aperture, the required accelerating voltage integrated over the structure is reduced approximately quadratically with increased operating frequency (harmonic number) of the linearizer. Thus, the required RF power will be also dramatically reduced with increasing operating frequency. After numerous optimizations, a Ka-band (36 GHz) linearizer was selected as a base line. A compact and cost-effective Ka-band RF power source capable of generating 2~3 MW peak RF power, 1kHz repetition rate, 1000 ns pulses is required to drive such a 36GHz linearizer [2]. Design efforts on a special Ka-band Gyro-Klystron solution are in progress [3]. For this device, the 150 kV, 50 A beam and solenoidal magnetic field of 1.5 T were selected. In its configuration, the RF power station (including modulator and

super-conducting solenoid) requires a sufficiently large space reservation. Thus, this station shall be located outside of the accelerator tunnel and connected to the linearizer via a long special Ka-band transfer line with reduced RF losses.

As an alternative, the compact and cost-effective Ka-band Multi Beam Klystron (MBK) is considered [4-7]. To avoid the needs for an insulation oil tank, the MBK operating voltage was selected to be 60kV, thus the device can be located in proximity of the linearizer in the accelerator tunnel. This choice leads to a large number of individual beams to safeguard the low perveance in order to achieve high enough RF power production efficiency. Therefore, the RF cavities in the bunching circuit shall use a higher order mode (HOM) to host all these beams [8,9]. In return, the focusing magnetic field required to confine all the beams is about 3 times lower than the one in the Gyro-klystron. The beam optics of a such a high frequency MBK is an additional challenge [10,11]. It shall provide the safe transport of the individual beam in a tiny beam channel of 2 mm diameter. The solution of the MB optics with a double compression beam [12] has been adopted and proven to be efficient for this application.

In Section II, after this introduction, the HOM issues in the coaxial cavities will be discussed. The novel concept and design of the RF power couplers and output RF window will be presented. In Section III, the beam-wave interaction analysis and optimization using a 1.5D disk code and benchmarking results using a 3D Particle-In-Cell (PIC) code will be presented. In Section IV, the multi beam optics design using 2D and 3D simulation tools will be introduced together with the final klystron layout and the performance summary. Conclusion will be made in Section V.

II. HOM RF CIRCUIT COMPONENTS

Operating high RF power devices at a beam voltage of 60kV and below, brings a significant advantage, as oil insulation will not be required. Thus, this value (60kV) was chosen as a starting point for the Ka-band MBK design. Other initial constraints for the design are the beam tunnel aperture and the beam filling factor. As a compromise between the cavity effective impedance and the expected single beam current, a beam tunnel of 2 mm diameter was selected. The individual beamlet current and the filling factor are constrained by the cathode loading and the amplitude of confining magnetic field. In order to achieve the required RF performance in the most practical way, a 6A current of each individual beamlet with a filling factor of 0.8 was adopted. With a gun area convergence of 40, the cathode loading will be less than $10A/cm^2$ (cathode radius R_c=4.7mm), and the magnetic field strength will be less than 0.6T (3~4 times the Brillouin magnetic field for the

Jinchi Cai (jinchi.cai@cern.ch) and Graeme Burt (graeme.burt@cockcroft.ac.uk) are with Department of Engineering of Lancaster University, LA1 4YW, Lancaster, United Kingdom; Igor Syratchev (igor.syratchev@cern.ch) is with BE/RF group at CERN (European Organization for Nuclear Research), Geneva, Switzerland.

immersive confinement). With such settings, the individual beam perveance is $0.4\mu A/V^{2/3}$. In general, such a low perveance should guarantee a rather high (>60%) RF power production efficiency [13,14]. However, after the preliminary studies, the expected efficiency was set to be rather conservative: 35%. Such an efficiency degradation is mostly driven by the intrinsically low impedance of the HOM cavities. Following the required level of the RF peak power production of 2.5 MW, 120A of total current was selected. That corresponds to a beamlets number of 20. To accommodate this large number of the beamlets at a such high frequency (cathode diameter is 1.12 times larger than the wavelength), a coaxial bunching cavity operated in the HOM $TM_{N,1,0}$ is a natural choice. The resonant frequency (f_0) of the $TM_{N,1,0}$ mode in a coaxial cavity, with the assumption that the beam tunnels do not distort the electric field distribution in the cavity, can be written as [15]:

$$\frac{2\pi f_0}{c} = \sqrt{\left(\frac{\pi}{a}\right)^2 + \left(\frac{\pi}{b}\right)^2}, a = \frac{2\pi r}{2N} \qquad (1)$$

here r is the median radius of the cavity and b is the radial width of the cavity. To ensure the electric field symmetry in the individual beamlet area, the additional constraint was introduced: $a=b$. To host N_b beams, the azimuthal index (N) of the operating mode shall be an integer harmonic (k=1, 2...) of N_b /2. With the field symmetry constrain, the cavity width shall satisfy the conditions: $k \times b > 2 \times R_c$. On the other hand, if all the conditions are satisfied for multiple modes, the preference shall be given to the operating mode with the lowest azimuthal index to maximize the impedance and the mode separation. Finally, we have selected the mode azimuthal index to be equal to the number of beamlets. For 36 GHz and $N=20$, $a=b=5.9$mm and the median radius of the cavity, $r=37.6$mm. This selection enables comfortable arrangement of the cathodes at the median radius, providing enough spacing between the cathodes. The well-known problem in any HOM device is a potential danger of the mode's competition [16]. The adjusted modes frequencies can be calculated using the simplified equation (1):

$$\frac{2\pi f_n}{c} = \frac{\pi}{b}\sqrt{\left(\frac{n}{N}\right)^2 + 1} \qquad (2)$$

Accordingly, the frequency of the mode with index $n=19$ is 35.11 GHz and with index $n=21$ is 36.911 GHz. However, with introduction of the beam tunnels into the cavity with a gap length of 1 mm, the situation is changed, so that the frequencies of the adjusted modes were shifted down in frequency: 34.7 GHz ($n=19$) and 36.39 GHz ($n=21$), see Fig 1 [17]. At the same time, the frequency of the cross polarized mode with $n=20$ was significantly detuned by -1.5 GHz. This modification still provides enough mode separation, especially for the idle bunching cavities, that are tuned up in frequency by about 100 MHz with respect to the operating frequency. Considering the higher frequency modes with indices $m \times N$ ($m=2,3$), their frequencies are not harmonics of 36 GHz (57 GHz; $n=40$). There are still more modes that can be considered dangerous, as far as they could satisfy both the spatial and the frequency harmonics synchronism [18]. Though, the possible effect of these modes will be studied by analyzing the results of the 3D PIC simulation in the next section.

The operating $TM_{20,1,0}$ mode in a cavity with gap length optimized for the highest effective impedance, delivers a relatively low beamlet impedance ($R/Q=1.4\Omega$). To compensate for that, the frequency tunings of the intermediate cavities shall be reasonably close to the operating frequency (about 100 MHz), so that the overall bandwidth of the device is relatively narrow (about 50MHz). Also, the external quality factor of the output cavity shall be rather high to compensate for the low impedance. Thus, the efficiency reach has to be negotiated between the beam deceleration and the Ohmic losses in the output cavity. To enhance the beam impedance, double-gap coaxial cavities operated in the 'π' mode were considered at one point. However, they have been discarded due to the very thin (<0.5 mm) separating wall between the cavities that is needed to support large enough '0' and 'π' mode separation [19,20]. Such a thin wall would have a rather low heat dissipation capability in the presence of fractional beam losses and Ohmic losses. That potentially could detune the operating mode due to wall deformation owning to its mechanical fragility.

To support the azimuthal symmetry of the electric field in the input and the output coaxial cavities, a distributed coupling concept with external waveguide laying around the cavity [21] was selected. In its initial configuration, the external wrap around waveguide was located outside the cavity and the power was extracted though the four orthogonal waveguides connected to the wrap-around waveguide. However, in this configuration, a complicated waveguide combination RF network will be required to collect the RF power into the single channel. That would also introduce the additional Ohmic losses. As a novel configuration, it was suggested to use internal waveguide ring (see Fig 2a). The proper choice of the internal ring width, the coupling slots width, and the width of the 4 orthogonal extracting waveguides support electric field symmetry and provide the required loaded quality factor. Apart from the operating mode, the additional volume of the inner ring will generate several coupled modes that are common to the ring and the cavity. It was found that the nearest mode is
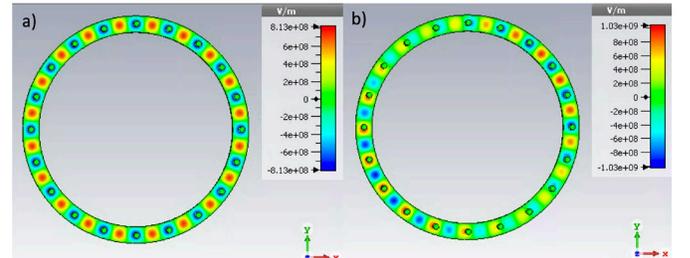
Fig. 1. $TE_{20,1,0}$ mode (a) and $TE_{21,1,0}$ mode (b) in the coaxial cavity with integrated beam tunnels.
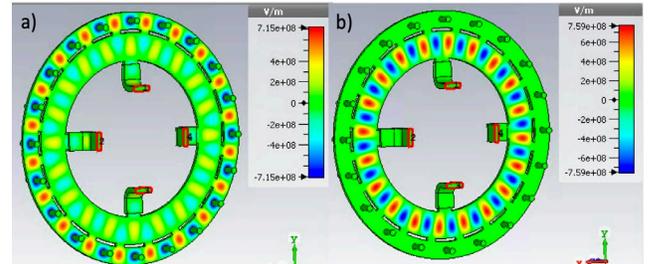
Fig. 2: The operating mode (a) and the nearest mode (b) in the output cavity with inner ring waveguide and 4 extracting waveguides.

separated by -250 MHz and the field pattern of this mode excludes its coupling to the beam (see Fig. 2b).

To combine the four output rectangular waveguides, we have used a mode conversion technique, where the four ports operated in the TE_{10} mode are combined into one rectangular waveguide operated in the TE_{20} mode and then finally, this mode is converted into the TE_{01} mode of the circular waveguide, see Fig. 3b. This technique requires orthogonal pairs of the 4 waveguides to operate with opposite RF phases. This was done by the gradual changing the width of each waveguides pair. Such a combination RF network is very compact and efficient. The RF transmission losses measured in HFSS simulations are below 0.1% [22]. This propagates the symmetrical TE_{01} mode of the circular waveguide, which is the most suitable for the design of the high-power RF vacuum window. The design of such a window with a traveling wave in the ceramic [23] is shown in Fig. 4. In this design the maximal value of electric field on the ceramic surface is below 10 MV/m at 3MW RF power. The input coupler is arranged in the similar way, but the TE_{20} mode is converted directly into the single rectangular waveguide operated in the $TE_{1,0}$, see Fig. 3a.
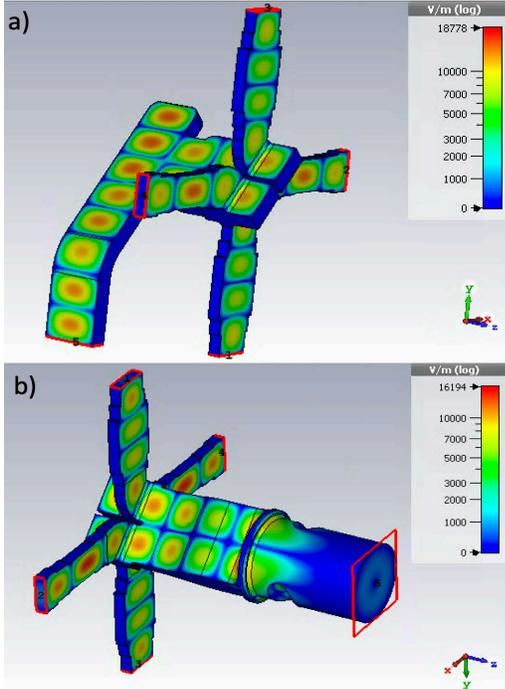
Fig. 3: Input (a) and output (b) combining RF networks of the HOM MBK.
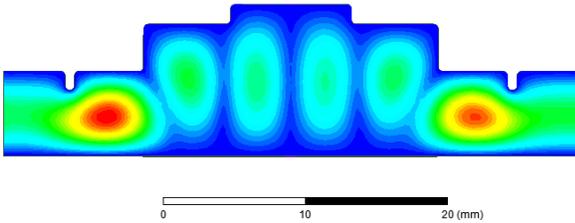
Fig. 4: The electric field plot in the 36 GHz, TE_{01} RF window with travelling wave in ceramic. The ceramic disc diameter is 21.8 mm.

III.   BEAM-WAVE INTERACTION SIMULATIONS

The RF bunching circuit of the HOM MBK was optimized with the KlyC/1.5 large signal klystron code [24]. The single beamlet environment with a 2D map of the electric field imported from CST/3D was used in these simulations. To ensure the best bunching quality, the Core Oscillation Method (COM) [25] was adopted for the bunching RF circuit design. The klystron comprises 8 cavities including the input and the output cavities. The cavities frequencies, positions and external Q factor of the output cavity were automatically adjusted by using the internal KlyC optimizer routine. With sparse cavities lateral distribution and resonant frequencies tuned up compared to the operating frequency, these tunings stratified the COM conditions [13]. The design goal was to optimize output power and hence efficiency of the MBK. Due to the low shunt impedance of the output cavity a high Q_e is required, hence limiting the bandwidth. As a result, no attempt was made to set the bandwidth as a design goal. The optimized tube (see Fig. 5) provided 33.3% efficiency (2.4 MW peak power), 50 MHz frequency bandwidth at a level of -3dB and the power gain of 40.7 dB. The obtained efficiency value can be compared to the electron efficiency of 49% measured in these simulations. This illustrates, that achieving the higher efficiency in a HOM MBK at such a high frequency is limited by the available impedance of the single gap cavity, so that the optimal external quality factor of the coupler in our case is almost 30% of the cavity intrinsic quality factor. If a technically feasible solution for the
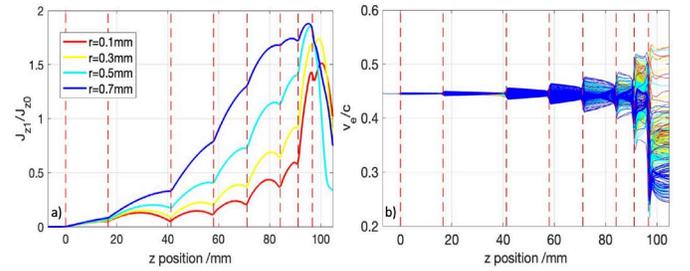
Fig. 5: KlyC simulation results: (a) current modulation depth at the different radii within the beamlet, (b) velocities modulation.
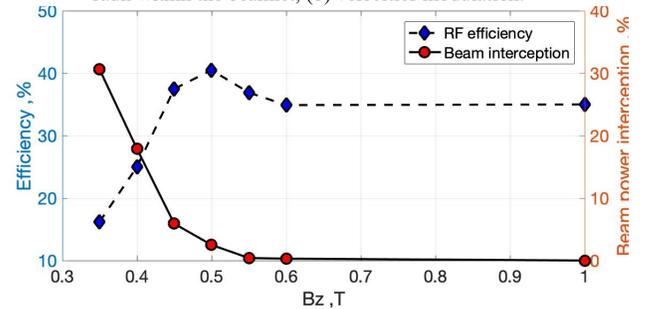
Fig. 6: The beam interception and klystron efficiency as functions of the solenoidal magnetic field strength measured in CST/3D PIC simulations.
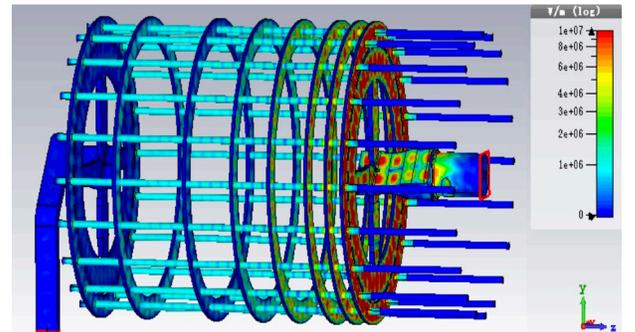
Fig. 7: The electric field plot on the HOM MBK surface.

double-gap HOM cavity design could be found, then the power production efficiency would be increased up to around 45% and the frequency bandwidth up to 150 MHz. The pulse-to-pulse RF phase stability is an important parameter for the linearizer operation. Modern modulators with IGBT technology provide HV pulsed stability at a level of 0.01%. This translates into the simulated RF phase jitter of the HOM MBK of ±0.38 degrees, which is below the specification of ±0.5 degrees RF phase for CompactLight.

Based on the KlyC recommendations, the full 3D model of the HOM MBK, including the input and the output RF combining networks, was generated and used in CST/3D PIC simulations. In these simulations, the 20 cylindrical 6 A beams of 1.6 mm diameter each were emitted from a metal surface with 60 keV energy. The homogenous solenoidal magnetic field was applied along the tube. First, the tube was successfully simulated in DC mode with a 2 microsecond long HV pulse to ensure the tube stability and absence of spurious monotron oscillations. Following, a number of simulations with different magnetic field amplitudes and 200 W of input RF power with a short pulse duration (200ns) were performed. One such simulation on the dedicated computer server equipped with 16 × 2.6GHz CPU cores, 256 GB memory and 2 × 12GB GPU cards takes 23 hours. It was observed (see Fig. 6), that the beam interception disappears, when the magnetic field amplitude exceeds the 0.55T and efficiency saturates at 35% (2.5 MW peak power). The lower value of the magnetic field provokes excessive beam radial expansion in the output cavity and thus the beam losses; hence these simulation results cannot be fully trusted at low magnetic field. An electric field plot on the klystron surface is shown in Fig. 7. For the extracted RF power of 2.5 MW, the maximal surface field in the output cavity is about 90 MV/m, which is below the target limiting value of 100 MV/m.

One of the critical issues of any HOM klystron is the potential danger of mode competition. In general, these modes can be synchronized with the beamlets number and the operating frequency harmonics. Moreover, if the current of the individual beamlets is not identical, the number of possible mode combinations will be increased. These effects were studied in a simulation of the klystron with one beamlet being switched off. The observed RF power reduction in this case was 7%. That is consistent with a reduction of 5% of the total current and a small
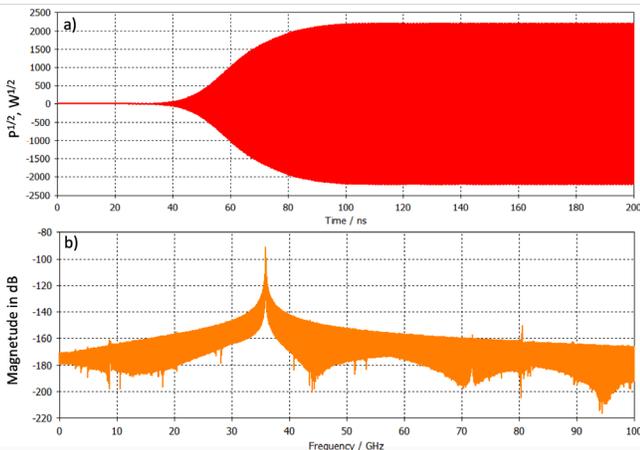
reduction in efficiency due to the change of the total perveance. The spectrum (up to 100 GHz) of the output RF signal (see Fig. 8) does not show any major frequency component apart from 36 GHz. We also may conclude, that with possible irregularities in the emission current of the individual beamlets, the RF power will respect the integrated current, whilst the irregularities pattern will not play a role.

The fabrication tolerances of 5 micrometres are well within reach in the modern diamond turning machines. With such fabrication tolerances, the cavity frequency errors will stay within 5 MHz, which is well below the klystron bandwidth of 50 MHz. Ultimately, after fabrication and brazing, the cavities tuning for exact frequency can be done using copper electro polishing and/or electro deposition technique. In operation, the klystron frequency control shall be done by regulating the temperature of the cooling water. Other RF circuit components, like the RF power combiners, are much less sensitive to the fabrication errors. For example, with 50 μm fabrication errors in the width in a single waveguide of the combiner, the simulated change of the combiner reflection stays below -17dB. This will affect the power production efficiency at a level of 0.1%.

IV. MULTI-BEAM OPTICS DESIGN AND OPTIMIZATION

To facilitate the fast and accurate simulations of the klystron's electron optics in 2D, dedicated computer tools were developed at CERN based on classic electro-static and magneto-static theory [26,27]. Together with KlyC/1.5 these tools, combined into the suit called CGUN, allow for the entire klystron simulation from the cathode to the collector. CGUN includes electro-static, magneto-static and beam tracking modules. CGUN was thoroughly benchmarked against DGUN/2D [28] and CST TRK/3D [17] and showed very good consistency.

For the HOM MBK, the cathode optics design with double beam compression [12] was adopted as a base line. This method
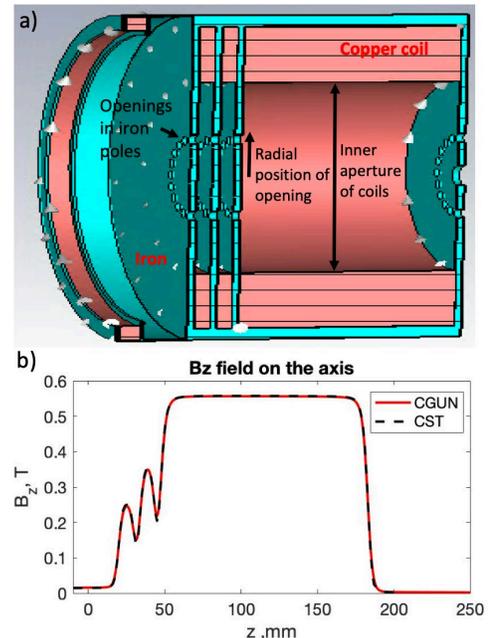
Fig. 9: The 3D layout of HOM MBK magnetic system (a) and magnetic field profiles simulated in CGUN and CST for the on axial beam (b).

Fig. 8: Output RF signal (a) and spectrum (b) for the case with one beamlet being switched off.

showed good potential for the MB cathodes. To provide the necessary magnetic field distribution along the beamlets trajectories, two short coils and one correction coil were added to the regular solenoid, see Fig 9a. Integrated iron poles are placed between each magnet allowing optimization of the local field around each interface. As a safe value, derived from the PIC simulations, the magnetic field amplitude in the solenoid was chosen to be 0.55T. First, the on-axial 2D single beam optics were optimized using CGUN. In this optimization the magnetic field profile was controlled by changing the current of three first coils. In Fig. 9b the magnetic field distribution simulated by CGUN and CST TRK/3D are compared. Both codes show good agreement, whilst CGUN is about 40 times faster than CST TRK/3D. As well as the magnetic field profile the cathode curvature and electrode spacing were used in the optimization to minimize the cathode loading and the beam scalloping. The beam trajectories in the final design of the single beam optics simulated by CGUN are shown in Fig. 10 together with the magnetic field profile and the current density distribution on the cathode surface, with a peak value of 8.9 A/cm^2. The CGUN results were verified by DGUN and CST TRK, see Fig.11. All three codes confirmed the stable beam transport with about 3% scalloping for the 6 A beam with 0.8 mm radius.

Analysis of the entire ensemble of the 20 beamlets optics was done using CST TRK/3D. The 3D map of magnetic field was provided from the separate CST simulations of the magnetic

system shown in Fig. 9. The initial beam tracking simulations showed dramatic beam losses (almost 40%) due to the presence of the magnetic field transverse component ($B_{\perp max}$=0.05T). To minimize $B_\perp$ on the beamlet axis, the inner aperture of the coils and radius of the openings in the iron poles (Fig. 9a) were optimized. When the inner radius of the coils is sufficiently large (97 mm), the aperture of the openings in the iron poles appeared to be the most sensitive parameter. With adjusting the openings radius to be 1.37 times larger than the radius of the beam tunnel in the area of the beam double compression, the amplitude of the magnetic field transverse component was reduced to 0.002T ($B_{\perp max}$< 3.6×10^{-3}×$B_{||}$). With these measures, the beam losses were reduced to 3%. The original radial position of the openings centres was aligned with the beam tunnels centres. Final tuning of the magnetic circuit was done by a small (0.15 mm) radial offset of the openings centres with fixed opening apertures (Fig. 9a), so that the beam transmission reached 100%, see Fig. 12 and Fig. 13. This later optimization was based on the direct TRK simulations. However, this last tuning caused a slight elliptical deformation of the beam cross-section, visible in Fig. 11, and the beam clearance at some points is reduced to about 0.1 mm. It shall be noted that the accurate simulation of such a complex optics in CST is very time consuming. 20 million mesh cells and 400×2 current emission sights were used in simulation. Thus, a limited number of parameters were used in the optics optimization at this stage. We believe that with more effort, further optimization can
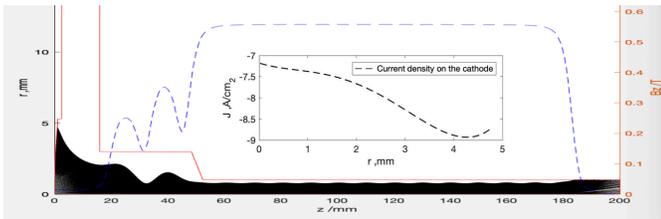
Fig. 10: 2D Beam trajectory simulated in CGUN shown together with magnetic field profile and the current density distribution on the cathode.
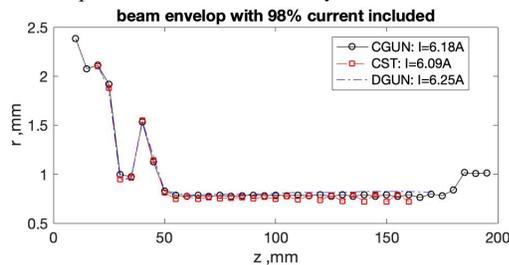
Fig. 11: Beam envelops simulated by the different codes.
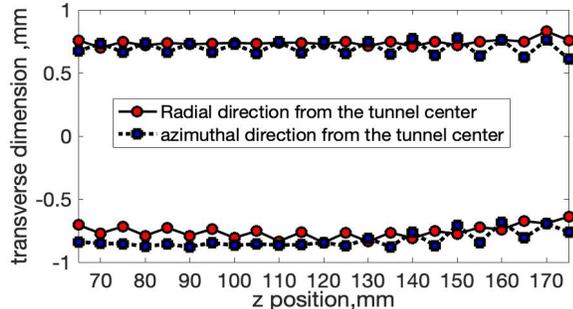
Fig. 12: Single beamlet TRK simulation with imported 3D magnetic field. Beam envelopes are shown for the region of the constant magnetic field.
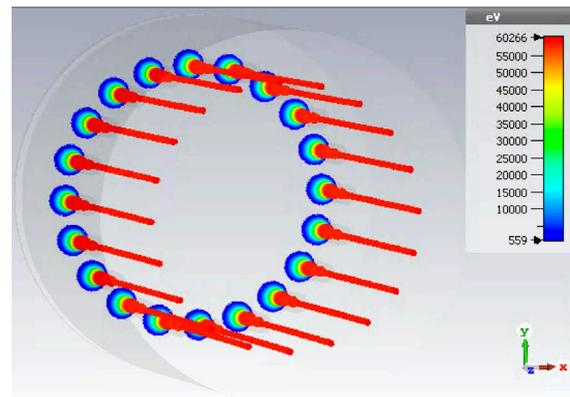
Fig. 13: MBK beams optics simulation in CST TRK/3D.
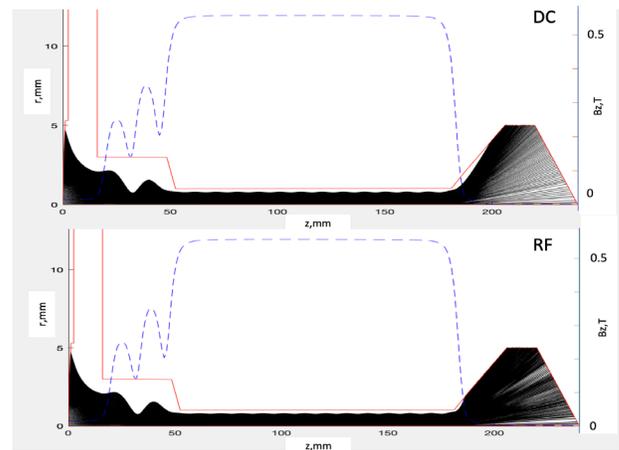
Fig. 14: The particles trajectories for the two operational regimes and optimized collector shape.
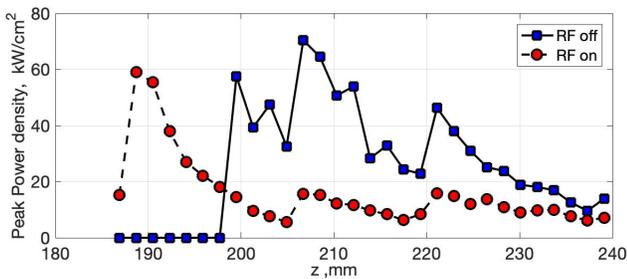
Fig. 15: The power dissipation density profiles on the collector surface.
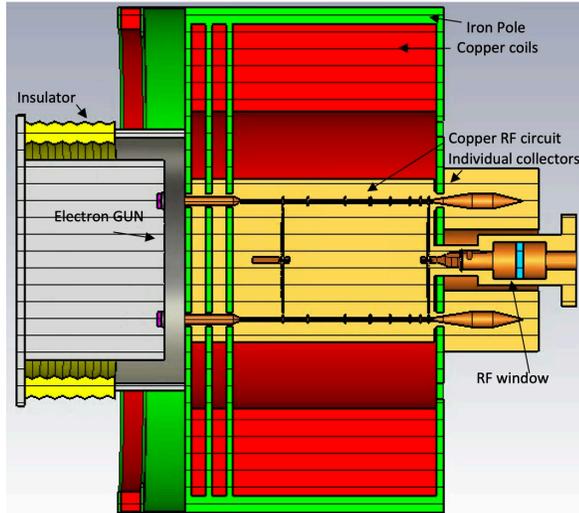
Fig. 16: Artistic view of the Ka-band HOM MBK.

TABLE I. Design parameters of the Ka-band HOM MBK

Parameter	Value	Unit
Operating frequency	36	GHz
Beam Voltage	60	kV
Total beam current	120	A
Number of beams	20	
Total perveance	8	$\mu AV^{-3/2}$
Perveance of the beamlet	0.4	$\mu AV^{-3/2}$
Peak RF power	2.5	MW
RF efficiency	35	%
Bandwidth (- 3dB)	50	MHz
Focusing magnetic field	0.55	T
Average cathode loading	8.2	A/cm^2
Pulse length	1000	ns
Repetition rate	1000	Hz
DC coil power consumption	~7	kW
RF circuit length	9.7	cm

improve the quality of the beam transport. To achieve the required focusing magnetic field of 0.55T, normal conducting copper coils can be used. We have calculated that total DC power consumption in all magnets will be about 7kW. With a conventional water cooling circuit, the estimated temperature rise of the solenoid will be 20 K^0. The coil power consumption will reduce the overall system efficiency by about factor 2. However, using this conventional technology is significantly less expensive than a superconducting magnet.

To increase the heat dissipating surface of the collector, it was

decided to use an individual mini collector for each beamlet. In this case the task is degenerated to a 2D environment and the CGUN code can be used as an appropriate tool for the collector optimization. CGUN has two options for the collector simulation: DC and RF regimes. If RF regime is chosen, a map of the radial distribution of electrons velocities in the spent beam is imported from KlyC and used in the particle tracking. If necessary, an additional option of secondary electron tracking can be activated as well. The particle trajectories for the two regimes and optimized collector shape are shown in Fig. 14. The power dissipation density profiles on the collector surface for the two regimes are compared in Fig. 15 for the operating point of the klystron running at 1 kHz repetition rate and 1 microsecond RF pulses. The maximal power density is below 70 W/cm^2. This is well below the conservative value of 100W/cm^2 typically used in collectors with a water cooling system.

The layout of the Ka-Band HOM is shown in Fig. 16. The overall klystron length is 0.37m and outer diameter is 0.33m. The tube parameters are summarized in Table I. The design of the cooling circuit, the fabrication technology (3D printing of the collector unit with integrated cooling circuit for example) and further optimization of the beam optics will be addressed in further studies.

V. CONCLUSION

Modelling, optimization, and design study of a compact and cost-effective 2.5 MW Ka-band HOM MBK was presented. To avoid the need for an insulation oil tank, the MBK operating voltage was selected to be 60kV, thus the device can be in proximity of the linearizer in the accelerator tunnel. The innovative concept of the output coupler with an integrated combination and mode conversion RF circuit allows for efficient RF power extraction and a robust vacuum RF window design. Detailed study of the beam-wave interaction and beam optics design confirmed that reliable operation of the MBK klystron operated in a HOM mode with a large azimuthal index is feasible. This technology can also be used at low frequency bands (C and X) for development of the very high, of the order of 100 MW, peak RF power devices operated at reduced HV level.

REFERENCES

[1] G.D'Auria, S. DiMitri, R. Rochow, et al. "CompactLight Design Study " in IPAC2019, Melbourne, Australia, 9-12 October 2019.
[2] A, Castilla, G. Burt, A. Latina, X. Liu, W.L. Millar, X. W, W. Wuensch, "Ka-band Linaerizer Studies for a compact Light Source", in IPAC2019, Melbourne, Australia, 9-12 October 2019.
[3] L. Wang, K. Dong, W. He, J. Wang, Y. Luo, A.W. Cross, K. Ronald, and A.D.R. Phelps , "Design of a Ka-band MW-level high efficiency gyroklystron for accelerators", IET Microwaves, Antennas & amp; Propagation, vol.12, no.11, pp.1752-1757.
[4] E.A. Gelvich, L.M. Borisov, Y.V. Zhary, A.D. Zakurdayev, A.S. Pobedonostev and V. I. Poognin, "The new generation of high-power multiple-beam klystrons", in IEEE Trans. on Microwave Theory Tech., vol.41, no.1, pp.15-19, Jan 1993.
[5] K.T. Nguyen, E.L. Wright, D.E. Pershing, D.K. Abe, J.J. Petillo, B. Levush, "Broadband High-Power 18-Beam S-band Klystron Amplifier", in IEEE Trans. on Electron devices, vol.56, no.5, pp.883-890, April 2009.

[6] D.K. Abe, D.E. Pershing, K.T. Nguyen, R.E. Myers, E.L. Wright, F.N. Wood, E.L. Eisen, I.A. Chernyavskiy and B. Levush, "Experimental Study and Analysis of an S-Band Multiple-Beam Klystron With 6% Bandwidth", in *IEEE Trans. on Electron devices*, vol.56, no.5, pp.846-854, May 2009.

[7] J.C. Cai and I. Syratchev, "Modeling and Technical Design Study of Two-Stage Multi-beam Klystron for CLIC", in *IEEE Trans. on Electron devices*, vol.56, no.5, pp.846-854, August 2020.

[8] A.N. Korolyov, E.A. Gelvich, Y.V. Zhary, A.D. Zakurdayev and V.I. Poognin, "Multiple-beam klystron amplifiers: Performance parameters and development trends", in *IEEE Trans. on Plasma Sci.*, vol.32, no.3, pp.1109-1118, Jun. 2004.

[9] Y.G. Ding, "Technological Progress on Multi-Beam Klystrons" AIP Conference Proceedings 807, 82 (2006).

[10] K, T. Nguyen, D. E. Pershing, D.K. Abe, G. Miram, B. Levush, "Eighteen-Beam Gun Design for High Power, High Repetition Rate, Broadband Multiple-Beam Klystron", in *IEEE Electron device letters*, vol.33, no.2, pp.270-272, April 2005.

[11] R. Zhang and Y. Wang, 'Six-Beam Gun Design for a high-power multiple-Beam Klystron', in *IEEE Electron device letters*, vol.38, no.6, pp.1337-1344, June 2010.

[12] A. Larionov, "Optical system of the powerful multi-beam L-band klystron for linear collider', 19th RuPAC, Dubna 2004, Russia, pp.456-458.

[13] J.C. Cai, I. Syratchev and Z. Liu, "Scaling Procedures and Post-Optimization for the Design of High-Efficiency Klystrons", in *IEEE Trans. on Electron Devices*, vol.66, no.2, pp.1075-1081, February 2019.

[14] Z.Liu, H. Zha, J. Shi, H. Chen, "Study on the Efficiency of Klystrons", in *IEEE Trans. on Plasma Science*, vol.47, no.4, pp.1734-1741, April 2019.

[15] K.Q. Zhang, D.J. Li.*Electromagnetic Theory for Microwaves and Optoelectronics,* China: Publishing House of Electronics Industry, 2001.

[16] D. Wang, G. Wang, J. Wang, S. Li, P. Zeng and Y. Teng, "A high-order mode extended interaction Klystron at 0.34THz", Physics of Plasmas, vol.24, no.023106, Feb. 2017.

[17] CST 2018. Available at: https://www.cst.com/products

[18] J.C. Cai, I. Syratchev, G. Burt, "Accurate Modeling of Monotron Oscillations in Small and Large Signal Regimes", in *IEEE Trans. on Electron Device*, vol.67, no.4, pp.1797-1803, April 2020.

[19] D. Zhao, W. Gu, X. Hou, G. Liu, Q. Xue and Z. Zhang, "Demonstration of a High-Power Ka-band Extended Interaction Klystron", in *IEEE Trans. on Electron devices*, doi:10.1109/TED.2020.3008881.

[20] Y.M. Shin, G. S. Park, G. P. Scheitrum and G. Caryotakis. "Circuit analysis of Ka-band extended interaction Klystron " in Proc. 4th IEEE Int. Conf. Vac. Electron., Seoul, South Korea, May 2003, pp. 108-109.

[21] E. Jensen and I. Syratchev, "CLIC 50 MW L-Band Multi-Beam Klystron", 7th International High Energy Density and High Power RF Workshop, Kalamata, Greece, 13-17th June 2005.

[22] HFSS 2018. Available at: https://www.ansoft/products/hf/hfss

[23] S. Yu. Kazakov, S. Michizono, H. Mizuno and Y. Saito, "RF High Power Test of the X-Band Windows with TWR", Proc of the International LINAC Conference, Tsukuba, Aug. 1994.

[24] J.C. Cai, I. Syratchev, "KlyC: 1.5D Large Signal Simulation Code for Klystrons", in *IEEE Trans. on Plasma Science*, vol.47, no.4, pp.1734-1741, April 2019.

[25] A. Yu. Baikov, C. Marrelli, I. Syratchev, "Toward High-Power Klystrons with RF Power Conversion Efficiency on the Order of 90%", in *IEEE Trans. on Electron devices*, vol.48, no.6, pp.2089-2096, Jun. 2020.

[26] Q.F. Li, .*Numerical calculation of electromagnetic fields and design of electromagnets,* China: Tsinghua University Press, 2002.

[27] W.B. Hermannsfeldt, "EGUN an electron optics and gun design program", SLAC Nat. Accel. Lab., Menlo Park, CA, USA, Tech. Rep. SLAC-331, Oct. 1988.

[28] A. Larionov, K. Ouglekov, "DGUN-code for simulation of intensive axial-asymmetric electron beams", 6th International Computational Accelerator Physics Conference, TU Darmstadt, German, 2000, p.172.